Surface tension of fully flexible Lennard-Jones chains: Role of long-range corrections

Luis G. MacDowell[1,a)] and Felipe J. Blas[2]
[1]*Departamento de Química-Física, Facultad de Ciencias Químicas, Universidad Complutense de Madrid, 28040 Madrid, Spain*
[2]*Departamento de Física Aplicada, Facultad de Ciencias Experimentales, Universidad de Huelva, 21071 Huelva, Spain*

(Received 2 June 2009; accepted 12 July 2009; published online 21 August 2009)

We have calculated the interfacial properties of fully flexible chains formed from tangentially bonded Lennard-Jones beads by direct coexistence. The full long-range tails of the potential are accounted for by means of inhomogeneous long-range corrections consisting in slice by slice summation of interactions away from the truncation sphere. We show that the corrections may be transformed into an effective long-range pair potential plus a self term, thus allowing for a fast and easy implementation of the method. After addition of the effective pair potential, the coexistence densities agree very well with results from Gibbs-ensemble simulations with usual homogeneous long-range corrections. We calculate the surface tensions without the need for explicit evaluation of the virial by using the wandering interface and test area methods. Comparison with surface tensions obtained previously for chains of truncated Lennard-Jones beads show a very large contribution of interactions beyond truncation radii as large as four bead diameters. The percentage change is about 40% for low temperatures but may increase beyond 60% for high temperatures, thus revealing the need for proper account of long-range corrections for models with untruncated interactions. The study of interfacial properties with chain length shows asymptotic increase for the surface tension and related asymptotic decrease for the interfacial width. © *2009 American Institute of Physics*. [DOI: 10.1063/1.3197009]

I. INTRODUCTION

The study of interfacial properties and surface tensions has attracted the attention of simulators over the years.[1–3] Actually, the very first few simulations of hard spheres where affected unexpectedly by interfacial phenomena.[4,5] The observation of a finite size loop upon compression was the signature of freezing and the appearance of a fluid-solid interface. Already in 1965 it was suggested that such finite loops could be exploited in order to estimate the fluid-solid surface tension of hard spheres.[6]

Despite the long history and great number of studies, calculation of surface tensions remains a subtle problem with many pitfalls. This includes the ambiguity in the definition of the pressure tensor,[1] the finite size effects due to capillary waves,[7] oscillatory behavior of interfacial tensions in small interfaces,[8] strong dependence on the procedure employed in truncating the virial,[9] and last but not least, the difficulty to account for the long-range contributions to the intermolecular potential.[10–16]

In simple bulk fluids, the truncation of the potential may be easily remedied by including well known long-range corrections.[2] For inhomogeneous fluids, however, the presence of an unknown density profile along the interface makes the evaluation of long-range forces much more problematic. For this reason, the corrections are ignored in most studies, and the results reported are those corresponding to the model that interacts through the truncated potential. However, this is known to have considerable effect in the surface tension. Very recently it has been shown that including long-range corrections will not only increase the surface tension, but may also help in avoiding some problems such as the oscillatory behavior discussed above.[17]

The strong effect of truncating the potential in the calculation of surface tensions was already noted by Chapela *et al.*[10] long time ago. These authors obtained results for a truncated Lennard-Jones (LJ) potential and evaluated corrections to the surface tensions by assuming a hyperbolic tangent density profile. The method was later on corrected by Blokhuis *et al.*[18] and applied by several authors.[19–21] Although the corrections may become very important, this method can only provide a lower bound to the surface tension, because it employs density profiles obtained from the untruncated system.

Another method devised for accounting interactions beyond cutoff was proposed by Guo and Lu.[12] These authors provided corrections to the internal energy, pressure, and surface tension without making any *a priori* assumption about the density profile. The long-range corrections are divided into two contributions. The first one is the most important and has the advantage of being strictly local, hence very easy to evaluate. The second one is smaller, but involves a nonlocal term that is usually neglected.[19,21,22] Applying the energy or force corrections on the fly produces the correct asymptotic vapor and liquid densities of the untruncated potential. Unfortunately, the nonlocal term can only be solved

a)Electronic mail: luis@ender.quim.ucm.es.

numerically, as it involves an integral over density differences which makes the procedure rather inconvenient for run time calculations. This seems to be of little consequence at low temperature but becomes important close to the critical point.[23]

The same conceptual device proposed by Guo and Lu[12] may be cast into a more tractable form by writing down the required integrals in cylindrical coordinates.[13,15,16,23,24] This was noticed by Mecke *et al.*[13,24] who calculated the long-range corrections to the force on a particle in their molecular dynamics studies of interfaces. Unfortunately, Mecke *et al.*[13,24] neglected the contribution to the force that arise from particles beyond the truncation sphere whose perpendicular distance to the interface is less than R_c (cutoff distance or radius). This problem was reflected in their algorithm as a failure to produce results independent of R_c at high temperatures.[23] Daoulas *et al.*[16] calculated explicitly correct expressions for the long-range contribution to the potential energy. Surprisingly, taking the gradient of the potential without extra care produces the same expression for the force as that obtained by Mecke *et al.*[13,24] The problem was revisited recently by Janeček *et al.*,[14,23] who obtained corrected expressions for the energy, the force, and the virial. Once all contributions were properly accounted for, the method was found to be very robust to the choice of cutoff radius.

An important shortcoming of the methods discussed so far is the introduction of a mean field approximation. Indeed, such methods assume a density profile that depends only on the perpendicular distance to the interface. Whereas this is obviously correct on the average, it is not exact as an assumption for instantaneous configurations, which may show surprisingly structured interfaces.[25] As a result, the method washes out capillary fluctuations that could be important close to the critical point.[1] If one is interested in such fluctuations, the long-range effects may need to be considered using a lattice summation technique for LJ potentials.[26] In practice, it seems that surface tensions obtained with the lattice summation are in good agreement with "mean field" approaches for the long-range corrections, but the calculations become considerably time consuming.[11,27]

In this work we exploit the long-range correction scheme of Mecke *et al.*,[13,24] Daoulas *et al.*,[16] and Janeček *et al.*[14,23] in order to asses the effect of truncation on the surface tension of short chain oligomers. This extends our previous work were the surface tension of chains interacting with a truncated LJ potential was calculated.[28] The surface tension of simple coarse grained chain molecules has been considered previously in several studies,[28–34] but in all such cases the potential was truncated beyond some cutoff distance. Potentially, the role of long-range contributions could be here more important than for simple atomic fluids, because we expect the interfacial width to be broader, at least when described in corresponding states.[28,35]

The surface tensions of LJ chains are calculated here with two recently proposed algorithms, the wandering interface method (WIM) (Ref. 36) and the test area method (TAM).[37] Both of the methods are related and share a very desirable feature, namely, there is no need for explicit evaluation of the pressure tensor. This is particularly advantageous in this case, where the long-range corrections to the virial may become complex. With the WIM or TAM methods, it suffices to add the corrections to the energy in the Monte Carlo (MC) Markov chain in order to obtain the corrected surface tensions directly from the simulations.

The remaining of the paper is organized as follows. In the next section we briefly describe the long-range corrections to the energy recently reported by Daoulas *et al.*[16] and Janeček,[14] and show how they can be transformed into an easy to program effective pair potential. In Sec. III we describe the simulation setup and methodology for calculating the surface tension. Section IV reports our results on the phase diagram and surface tensions of the fully flexible LJ chains, while a final section summarizes our conclusions.

II. EFFECTIVE LONG-RANGE PAIR POTENTIAL

Consider a system of N molecules contained in a volume V that interacts through a pairwise intermolecular potential. The energy felt by species i due to interactions beyond the cutoff distance may be expressed in terms of the instantaneous density profile as

$$U_i^{lrc} = \int_{V \ni \mathfrak{S}(R_c,\mathbf{r}_i)} \rho(\mathbf{r}) u(\mathbf{r}_i,\mathbf{r}) d\mathbf{r}, \tag{1}$$

where R_c is the cutoff radius, $u(\mathbf{r}_i,\mathbf{r})$ is the intermolecular potential between two molecules located at $\mathbf{r}_i$ and $\mathbf{r}$, respectively, $\rho(\mathbf{r})$ is the number density at $\mathbf{r}$, and $\mathfrak{S}(R_c,\mathbf{r}_i)$ is a sphere of radius R_c centered in $\mathbf{r}_i$. In a mean field sense the density profile is a function of z only, so that the volume integration is best performed as a sum over parallel slabs

$$U_i^{lrc} = \int_{-\infty}^{\infty} \rho(z) \left\{ \int_{A \ni \mathfrak{C}(r_\parallel^{\min},z_i)} u(\mathbf{r}_i,\mathbf{r}) d\mathbf{r}_\parallel \right\} dz, \tag{2}$$

where $\mathfrak{C}(r_\parallel^{\min},z_i)$ is a circle of radius $r_\parallel^{\min}$ centered at z_i. $r_\parallel^{\min} = (R_c^2 - (z-z_i)^2)^{1/2}$ for $R_c^2 > (z-z_i)^2$ and 0 otherwise.

For the special case of the LJ potential, the term in brackets may be integrated right away using cylindrical coordinates, leading to

$$U_i^{lrc} = \int_{-\infty}^{\infty} \rho(z) w(z-z_i) dz, \tag{3}$$

with

$$w(z) = \lim_{l^2 \to \max(R_c^2 - z^2, 0)} 4\pi\sigma^2\epsilon \left[\frac{1}{5} \left(\frac{\sigma^2}{l^2+z^2} \right)^5 - \frac{1}{2} \left(\frac{\sigma^2}{l^2+z^2} \right)^2 \right], \tag{4}$$

where σ and ϵ are the units of distance and energy of the LJ intermolecular potential, respectively. The above equation is the long-range correction for the internal energy obtained by Daoulas *et al.*[16] and Janeček.[23] The result includes non vanishing contributions for slabs at distances less than R_c which where implicitly neglected in the corrections to the force previously employed by Mecke *et al.*[13,24] Obviously, the above equation could have been written as a simple piecewise function. We have purposely chosen to write it as above

to stress that the correct long-range force may be obtained as a gradient of this potential only when the gradient operator is performed *prior* to the limit $l^2 \to \max(R_c^2 - z^2, 0)$. Taking the gradient of the potential after the limit erroneously suggests null force for $|z| < R_c$. This subtle point arises due to the z dependence of the limits of integration required to obtain $w(z)$ [cf. Eq. (2)]. The correct expression for the force may be also calculated as in Eq. (2), with u substituted by ∇u.[14]

The total energy arising from long-range corrections is given as a sum over individual contributions, with a factor of 1/2 not to include mutual interactions twice

$$U^{lrc} = \frac{1}{2}\sum_{i=1}^{N} \int_{-\infty}^{\infty} \rho(z) w(z - z_i) dz. \tag{5}$$

The above expression may be evaluated by discretization of the z coordinate and evaluation of the density inside slices centered at nodes z_k.[14,16,23,27,38] If the density profile is updated on the fly during the simulations, the calculation of the long-range corrections may be performed very efficiently. The procedure, however, turns out to be cumbersome in the case of molecular systems, where each displacement will involve changes in the long-range corrections of all molecular sites. The book keeping device is then lengthy to program and requires extensive changes in the computer code (cf. Ref. 16). In order to circumvent this problem, the above equation may be rewritten as a sum of pairwise interactions. This can be achieved by recalling

$$\rho(z) = \frac{1}{\mathcal{A}}\sum_{j=1}^{N} \delta(z - z_j), \tag{6}$$

where $\mathcal{A}$ is the interfacial area of the $x-y$ plane, $\delta(z-z_j)$ represents the δ-Dirac function, and z_j is the z coordinate of molecule j. Substitution of this equation into Eq. (5), followed by integration along z yields:

$$U^{lrc} = \frac{1}{2\mathcal{A}}\sum_{i=1}^{N}\sum_{j=1}^{N} w(z_j - z_i). \tag{7}$$

The unrestricted summation over i and j indices can be finally transformed into a sum of pair and *self* terms:

$$U^{lrc} = \frac{1}{\mathcal{A}}\sum_{i=1}^{N-1}\sum_{j=i+1}^{N} w(z_j - z_i) + \frac{1}{2\mathcal{A}}\sum_{i=1}^{N} w(0). \tag{8}$$

This result corresponds to the exact evaluation of Eq. (5) with no need for discretization. Surprisingly, it corresponds to the addition of an extra effective pair potential evaluated within the minimum image convention along the z direction. Furthermore, the above expression has some desirable features. It is easily implemented within a computer code and does not need on the fly evaluation of density profiles. Obviously, the long-range nature of this potential makes the procedure time consuming. Our calculations show that simulation of a system with $R_c = 3\sigma$ plus long-range corrections as in Eq. (8) takes about the same time than the simulation of the bare LJ potential with truncation at $R_c = 4\sigma$. Note that as long as the surface area remains unchanged, the self term is a constant. Hence, attempted displacements will only involve the effective pair interactions. On the contrary, changes in the self term must be accounted for when the simulation box is deformed.

III. MODEL AND SIMULATIONS

Our model polymers consists of a chain of m bonded interaction sites. The interaction sites are of the LJ type

$$U(r_{ij}) = \begin{cases} 4\epsilon\left[\left(\frac{\sigma}{r_{ij}}\right)^{12} - \left(\frac{\sigma}{r_{ij}}\right)^{6}\right] & r_{ij} \le R_c, \\ 0 & r_{ij} > R_c, \end{cases} \tag{9}$$

where σ and ϵ are the units of distance and energy, respectively, and r_{ij} is the distance between monomers i and j. Successive LJ beads within a chain are flexibly constrained to a fixed bond distance of σ. In other words, the fully flexible tangent LJ chains model has neither bending nor torsional potentials between the monomers in a chain, although there is an *intramolecular* pair interaction between monomers of the same chain separated by more than one bond.

In our previous work (Ref. 28) we have studied chains where the LJ potential was truncated at $R_c = 3$, 4 and 5σ. In this study we will obtain results for the full LJ potential, i.e., corresponding to infinite truncation distance.

Simulations were performed in a tetragonal box with a liquid slab surrounded by the vapor phase. The box dimensions parallel to the liquid slab was set to $L_x = L_y$, with $L_x = L_y = 11\sigma$. The dimension perpendicular to the interface was chosen such as to accommodate the liquid phase and a large amount of vapor phase, with L_z between 72 and 90 molecular diameters long. We have studied chains of length $m = 4$, 8, 12, and 16 and the number of molecules (N) in the simulations determined so as to accommodate a total of 2016 monomers. Initial configurations were obtained from our previous study of truncated LJ chains,[28] and then allowed to equilibrate with the long-range interactions switched on. In both equilibration and production stages the interactions were evaluated explicitly up to $R_c = 3\sigma$, with the remaining contribution of the potential determined with the effective potential described in the previous section.

Sampling of configurational space was performed by means of a configurational bias MC code, with details described elsewhere.[28,39,40] The simulations were organized in cycles. Each cycle consists in N trial MC moves. We performed center of mass displacements, as well as partial and total configurational bias chain regrowth.[41] Each type of move is chosen with a probability of 20%, 40%, and 40%, respectively. The magnitude of the appropriate displacements are adjusted so as to get an acceptance rate from ~30% to 50%. We use periodic boundary conditions in all three directions of the simulation box.

Surface tensions were calculated using either the WIM (Ref. 36) or TA (Ref. 37) methods. In neither of these methods is the virial required. Rather, the surface tension calculations were determined by evaluating the free energy cost of attempted deformations, as determined from the Boltzmann factor (hence, only the Hamiltonian is required for assessing the surface tension). The difference between the two methods lies in the strategy for attempting deformations.

In the WIM method, deformations of the simulation box at constant volume are attempted, and either accepted or rejected according to the Metropolis scheme. Since the system will spontaneously deform so as to decrease the interfacial area, a simple weight function brackets the range of allowed deformations. The surface tension may be calculated from the analysis of the surface area probability distribution, $P(\mathcal{A})=\exp(-\beta\gamma\mathcal{A})$, by either least square fit of $\ln P(\mathcal{A})$ or from the average of $\mathcal{A}$. Whereas in the original proposal of the WIM method the surface area was sampled continuously,[36] sampling over a discrete set of surface areas is also possible.[42] The WIM method is very robust, as it can be employed for the calculation of continuous and discontinuous model potentials alike. Results have been obtained for the surface tension of LJ and square-well fluids,[43] LJ dimers,[42] and LJ chains,[28,36] as well as for fluid-wall interfacial tensions of tangent hard sphere and LJ chains.[36]

In the TAM method, the sampling is performed in a box of fixed shape, but forward (positive surface increment) and backward (negative surface increment) "*test area*" deformations at constant volume are performed every cycle. Similar to the Widom test for particle insertions, the Boltzmann factor $\exp(-\beta\Delta U)$ associated to the test deformation is collected and the surface tension is readily calculated from their average.[37] Note that the Markov chain is not affected by the test deformations, so that the sampling is performed for a box of fixed shape. The TAM method has been used for the calculation of surface tensions of LJ fluids,[37] the Gay–Berne model,[37] different water models,[20] other simple molecules and alkanes,[21,22] as well as LJ chains.[28]

For each chain length, we perform simulations of inhomogeneous systems at different temperatures where vapor-liquid equilibrium is expected. We typically consider either six or seven temperatures in the range $\sim 0.5T_c$ up to $\sim 0.9T_c$, where T_c is the critical temperature of the system. Averages of density profiles are determined over a period of 2×10^6 MC cycles. The surface tension, however, is a magnitude that fluctuates much more than other thermodynamic and structural properties, such as internal energy, density profile, or vapor pressure. In order to obtain a better statistics, the surface tension is determined over a longer period of 8×10^6 MC cycles. The production stage is divided into M independent blocks. The ensemble average of the surface tension is given by the arithmetic mean of the block averages and the statistical precision of the sample average is estimated from the standard deviation in the ensemble average from $\bar{\sigma}/\sqrt{M}$, where $\bar{\sigma}$ is the variance of the block averages.

All the quantities in our paper are expressed in conventional reduced units, with σ and ϵ being the length and energy units, respectively. Thus, the temperature is given in units of ϵ/k_B, the density in units of σ^{-3}, the pressure in units of ϵ/σ^3, the surface tension in units of ϵ/σ^2, and the interfacial thickness in units of σ.

IV. RESULTS

We have followed the same analysis and methodology than in our previous work. The equilibrium density profiles $\rho(z)$ are computed from averages of the histogram of densities along the z direction over the production stage. Once $\rho(z)$ is known, coexistence densities and interfacial thickness are calculated from the analysis of the density profiles of each chain length and at each temperature studied. The critical temperature T_c and density ρ_c are also obtained using the simulation results of the vapor and liquid coexistence densities (Table I) and the universal scaling relation for the width of the coexistence curve

$$\rho_L-\rho_V=A(T-T_c)^{\beta}, \tag{10}$$

and the law of rectilinear diameters

$$\frac{\rho_L+\rho_V}{2}=B+CT. \tag{11}$$

A, B, and C are constants, and β is the corresponding critical exponent. A universal value of $\beta=0.325$ is assumed here.[1] Further details on the methodology employed may be found in our previous work.[28]

We have checked the consistency of the long-range corrections in two ways. First, we performed bulk NVT simulations with inhomogeneous corrections switched on and found that the results agreed with similar simulations with the usual bulk long-range corrections.[44] Second, we analyzed the coexistence densities of the equilibrated orthogonal simulation boxes presented in Table I, and found that they showed good agreement with previous Gibbs ensemble simulation results obtained by Escobedo and de Pablo.[45] A comparison of these results is shown in Fig. 1 for chains 4, 8, and 16 monomers long. Good agreement is found in all cases, although the comparison for $m=16$ is somewhat less good. We attribute the difference to the use of a bead spring model in the work of Escobedo and de Pablo.[45] Apparently the bond flexibility starts having a small but noticeable effect above $T=2.5$. Despite the small differences mentioned, we believe this comparison to be a convincing test of consistency for the inhomogeneous long-range corrections. Similar consistent results have been found in previous applications of the method.[23,27,38]

The role of long-range corrections may be anticipated by taking a look at the evolution of interfacial profiles as the cutoff radius is increased. Figure 2 shows density profiles for eightmers at two different temperatures as R_c is increased from 3–5 and up to infinity by virtue of the long-range corrections. The liquid densities increase and the vapor densities decrease as the range of the interactions become larger, thus increasing the segregation.

A. Phase equilibria

Figure 3 shows the coexistence curve obtained in this work for all the chains studied. As usual, the coexistence densities fall in the same scale when plotted as a function of monomer density. Furthermore, the trend in liquid coexistence densities suggests chain length independence for sufficiently long chains at low temperatures. This kind of behavior may be explained using Wertheim's thermodynamic perturbation theory,[46] as shown elsewhere.[47] The critical temperature increases with chain length for the moderate chain lengths studied here, but it is expected to attain a con-

TABLE I. Liquid density ρ_L, vapor density ρ_V, surface tension γ, and vapor pressure p, at different temperatures for systems of fully flexible LJ chains formed from m monomers with a segment-segment LJ cutoff of $r_c=3\sigma$ and inhomogeneous long-range corrections. The surface tension is calculated using the TAM and WIM methodologies. All quantities are expressed in conventional reduced units as explained in Sec. III. The errors are estimated from the standard deviation of the mean. In the case of the surface tension, this is obtained from 80 subaverages, each consisting of 10^5 cycles. In the case of ρ_L and ρ_V, we use the values of the equilibrium density profile corresponding to the liquid and vapor regions, respectively. For the vapor pressure, the errors are estimated using the synthetic analysis proposed recently by de Miguel, with a total of 4×10^6 synthetic data sets generated according to the prescriptions given by de Miguel (Ref. 42).

m	T	ρ_V	ρ_L	p	γ
4	1.0	0.000 008(1)	0.860(4)	0.000 002(5)	1.24(2)
4	1.2	0.0002(1)	0.806(2)	0.000 06(5)	1.01(2)
4	1.4	0.001 21(6)	0.751(1)	0.000 42(5)	0.778(9)
4	1.6	0.005 40(7)	0.6919(6)	0.002 03(5)	0.551(9)
4	1.8	0.0171(1)	0.6259(5)	0.006 68(7)	0.359(6)
4	1.9	0.0281(1)	0.5879(4)	0.010 84(6)	0.269(4)
4	2.0	0.0452(3)	0.5543(3)	0.0168(2)	0.191(3)
8	1.6	0.000 12(6)	0.739(2)	0.000 02(2)	0.779(14)
8	1.8	0.0008(2)	0.688(1)	0.000 18(9)	0.604(11)
8	2.0	0.0035(1)	0.635(1)	0.000 83(5)	0.441(10)
8	2.2	0.0111(2)	0.5764(7)	0.002 71(9)	0.287(8)
8	2.4	0.0301(6)	0.5057(7)	0.0070(2)	0.174(5)
8	2.5	0.0492(9)	0.4605(6)	0.0107(2)	0.118(4)
12	1.8	0.000 05(1)	0.708(3)	0.000 007(3)	0.70(2)
12	2.0	0.000 42(3)	0.658(2)	0.000 07(1)	0.54(1)
12	2.2	0.002 03(8)	0.609(1)	0.000 36(3)	0.41(1)
12	2.4	0.007 07(9)	0.5536(9)	0.001 29(3)	0.282(9)
12	2.6	0.0205(2)	0.4879(8)	0.003 64(6)	0.174(7)
12	2.7	0.0338(4)	0.4487(6)	0.005 67(9)	0.131(6)
16	2.0	0.000 007(1)	0.669(2)	0.000 0009(2)	0.59(3)
16	2.2	0.000 4(2)	0.624(1)	0.000 05(5)	0.47(3)
16	2.4	0.002 09(5)	0.572(1)	0.000 30(1)	0.31(2)
16	2.6	0.007 24(7)	0.5175(7)	0.001 07(2)	0.23(1)
16	2.7	0.012 49(7)	0.4859(5)	0.001 83(2)	0.20(1)
16	2.8	0.0217(2)	0.4507(2)	0.003 05(4)	0.16(1)

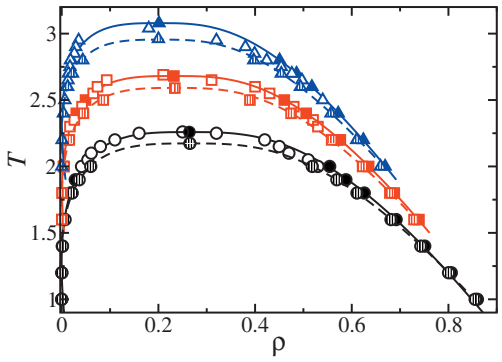

FIG. 1. Vapor-liquid coexistence density for fully flexible LJ chains. The circles, squares, and triangles correspond to the coexistence densities obtained from the analysis of the equilibrium density profiles obtained from Monte Carlo NVT simulations, for chain lengths of $m=4$, 8, and 16, respectively. The filled symbols correspond to chains interacting with a full LJ potential (including inhomogenous long-range corrections) studied in this work, shaded symbols to chains interacting with a segment-segment LJ cutoff distance of $r_c=4\sigma$ (without long-range corrections), and open symbols to chains interacting with homogenous long-range corrections taken from Ref. 45. The curves represent the fits of the simulation data to Eq. (10), and the symbols at the highest temperature for each chain length to the corresponding critical points estimated from Eqs. (10) and (11).

stant value asymptotically as $1/m$.[43] In order to study this point further we estimated the critical points of the LJ chains by extrapolation of scaling relations and the law of rectilinear diameters (cf. Ref. 28 for further details). We note at this point that more accurate estimates of the critical point may be obtained from finite size scaling techniques.[48,49] Unfortunately, the inhomogeneous long-range corrections that are applied incorporate to some extent a mean field character to the model, and the nature of the scaling behavior is then not quite clear.

Table II collects our estimated results for critical temperature and density. The results for the critical temperature where extrapolated to infinite chain length by means of a Flory–Schultz plot (not shown here), suggesting and asymptotic *theta* temperature of about $\Theta=4.36$, somewhat higher than the extrapolated theta temperature obtained from the results of Ref. 45, $\Theta=4.25$. According to Wertheim's thermodynamic perturbation theory of first-order (TPT1),[46,50] the theta temperature of chain molecules may be obtained by equating monomer and dimer-monomer virial coefficients.[51] From this analysis, a Theta temperature of $\Theta=4.92$ is predicted for LJ chains. On the other hand, using TPT1 from parametrized simulation data,[52,53] yields the *improved* result

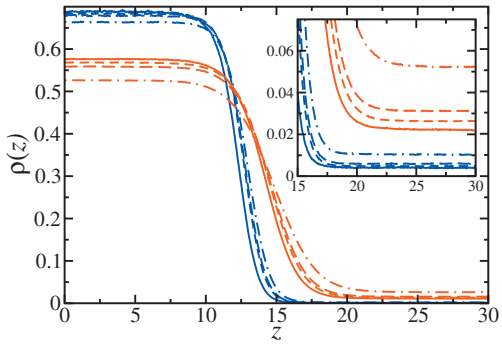

FIG. 2. Simulated equilibrium density profiles across the vapor-liquid interface of fully flexible LJ chains formed from eight monomers ($m=8$), at $T=1.8$ (blue curves) and $T=2.2$ (red curves) with a segment-segment LJ cutoff distance of $R_c=3\sigma$ (dotted-dashed curve), $R_c=4\sigma$ (long-dashed curve), $R_c=5$ (short-dashed curve) and for the full LJ potential with $R_c=3$ and inhomogeneous long-range corrections (full line). In the inset, the density profiles are presented to show the asymptotic approach toward the vapor phase, with results for $T=1.8$ and $T=2.2$ blown up a factor of 5 and 2, respectively.

$\Theta=4.65$ due to fortuitous cancellation of errors in the description of the reference state.[51]

Together with the simulation results for the liquid-vapor coexistence, we show predictions from two different equations of state based on the TPT1 approach. TPT1-MSA (Ref. 43) uses a LJ reference state with properties described from an analytic mean spherical approximation (MSA).[54] Soft-Saft-D uses LJ dimers as a reference state, and properties described by means of a parametrization to monomer and dimer simulation data.[55,56] As observed in Fig. 3, both TPT1 approaches provide a very good description of the results, except for the neighborhood of the critical point.

Calculation of the coexistence pressures poses some difficulties. For a model of fixed bond lengths as the one studied here, the expression for the virial is awkward, particularly for long chains whose end to end distance may be larger than half the simulation box.[57] This problem notwithstanding, acquisition of meaningful averages for such low pressures as are typical well below the critical point requires very lengthy simulations. For that reason, we calculated the pressure by means of a thermodynamic integration hinted at previously.[58] In this procedure we exploit the Gibbs–Duhem equation, $dp=\rho d\mu$, at constant temperature. By splitting the chemical potential into ideal gas and residual contributions, and integrating by parts, we obtain

$$\beta p(\rho) = \rho - \int_0^\rho [\mu_r(\rho') - \mu_r(\rho)] d\rho' . \tag{12}$$

In order to exploit this equation for the calculation of the pressure, we performed a series of bulk simulations in the grand-canonical ensemble. As in the case of the inhomogeneous system, we have also organized these simulations in cycles. As before, each cycle consists in N trial MC moves. The only difference is that we do not perform full chain configurational bias regrowth but grand-canonical configurational bias chain insertion/deletion. Each type of move is chosen with a probability of 20%, 40%, and 40% for center of mass displacements, partial configurational bias chain regrowth, and Grand-canonical configurational bias chain insertion/deletion, respectively. Typically, we run between 10 and 20 thermodynamic states from the ideal gas limit to the supersaturated vapor. Each state is equilibrated for 5×10^4 MC cycles, and averages of density are determined over a further period of 4×10^5 MC cycles. The production stage is divided into M blocks. We consider $M=50$ for all the states (different chemical potentials and temperatures) and chain lengths considered here. With this choice, the density at each chemical potential has been obtained from an average of 50 uncorrelated or statistically independent blocks (8×10^3 cycles per block). The residual chemical potential, as a function of density, was then fitted to a polynomial of second up to fifth order and integrated up to the coexistence vapor density. We have checked that our fitting procedure is essentially independent of the degree of the polynomial fit. Once the function $\mu_r=\mu_r(\rho)$ has been obtained, the vapor pressure can be readily calculated from Eq. (12). The statistical uncertainty associated with the thermodynamic integration of the equation of state given in Eq. (12) has been estimated from the *synthetic analysis* proposed recently by de Miguel.[42] In particular, we have generated 10^6 synthetic data sets according to the de Miguel's prescription,[42] obtaining a Gaussian-like distribution for the vapor pressure at each temperature. Our final results, including the statistical uncertainty of vapor pressure are presented in Table I.

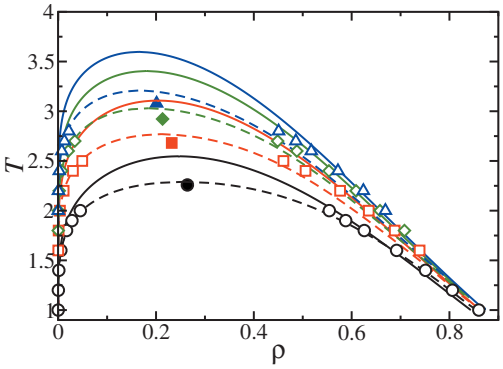

FIG. 3. Vapor-liquid coexistence density for fully flexible LJ chains with a segment-segment LJ cutoff of $R_c=3\sigma$ and inhomogeneous long-range corrections. The open circles, squares, diamonds, and triangles correspond to the coexistence densities obtained from the analysis of the equilibrium density profiles obtained from Monte Carlo NVT simulations, for chain lengths of $m=4$, 8, 12, and 16, respectively. The filled symbols are the corresponding critical points estimated from Eqs. (10) and (11), and the curves are the predictions from TPT1-MSA (continuous curve), and Soft-SAFT-D (dashed curves).

TABLE II. Critical temperature T_c and density ρ_c and the corresponding estimation of their errors, obtained from the analysis of the coexistence densities using the simulation results of the vapor and liquid coexistence densities (Table I) and Eqs. (10) and (11). All the chains formed from m monomers with a segment-segment LJ cutoff of $r_c=3\sigma$ and inhomogeneous long-range corrections. All quantities expressed in reduced units.

m	T_c	ρ_c
4	2.26(1)	0.264(7)
8	2.68(2)	0.23(1)
12	2.92(2)	0.21(1)
16	3.08(2)	0.20(1)

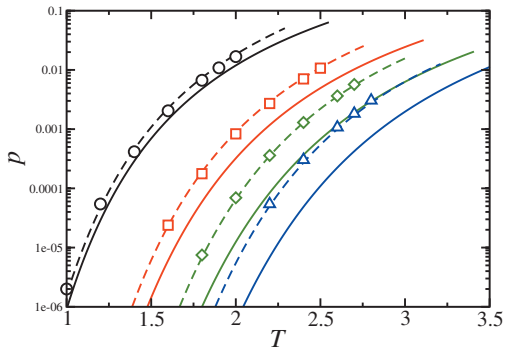

FIG. 4. Vapor pressure for fully flexible LJ chains with a segment-segment LJ cutoff of $R_c=3\sigma$ and inhomogeneous long-range corrections. The open circles, squares, diamonds, and triangles correspond to the coexistence densities obtained from the thermodynamic integration analysis explained in Sec. IV. A for chain lengths of $m=4$, 8, 12, and 16, respectively. The full lines are the predictions from TPT1-MSA, and the dashed lines from Soft-Saft-D.

Figure 4 shows the simulation results obtained for the vapor pressure of the chains studied. The results are compared also with TPT1-MSA and Soft-SAFT-D. TPT1-MSA shows good agreement for the vapor pressure of tetramers but very much deteriorates as the chain length is increased. On the contrary, the accurate description of the improved reference state (i.e., dimers instead of monomers) in the case of Soft-SAFT-D provides a rather good description of the vapor pressure for all chain lengths.

B. Interfacial properties

Figure 5 shows the results obtained for the surface tension of LJ chains as a function of temperature for chain lengths $m=4$, 8, 12, and 16. Results are shown for LJ chains with interactions beyond $R_c=3$ evaluated by means of the inhomogeneous long-range corrections, as well as for chains with LJ interactions truncated at $R_c=4$. Clearly, the long-range interactions play a very significant role, increasing the surface tension by a large amount both at low and high temperatures. A similar large effect was already noted long time ago for a glassy polymer-vacuum interface by Mansfield and Theodorou.[15]

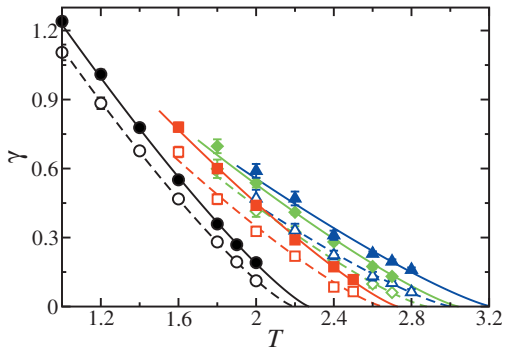

FIG. 5. Surface tension as a function of temperature for fully flexible LJ chains. The circles, squares, diamonds, and triangles correspond to the surface tension for chain lengths of $m=4$, 8, 12, and 16, respectively. The filled symbols correspond to chains interacting with a full LJ potential (including inhomogenous long-range corrections) studied in this work, and the open symbols to chains interacting with a segment-segment LJ cutoff distance of $r_c=4\sigma$ (without long-range corrections). The curves represent the fits of the simulation data to the scaling relationship of the surface tension near the critical point with $\gamma=\gamma_0(T-T_c)^{\mu}$ and $\mu=11/9$.

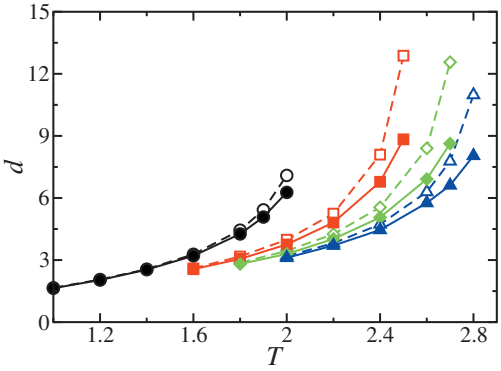

FIG. 6. The 10–90 interfacial thickness d as a function of the temperature for fully flexible LJ chains. The meaning of the symbols is the same as in Fig. 5. The curves are included as a guide to the eyes.

One may think right away of two reasons why the long-range corrections could result in such a large increase in the surface tension. First, for a given density profile, taking into account the interactions beyond some finite R_c will increase the energy difference between liquid and vapor phases. Second, including long-range corrections could distort the interfacial profile, further modifying the surface tension. The distortion of the density profile occurs in two ways. (1) The different treatment of LJ interactions could result in different bulk vapor and liquid densities. Figures 1 and 2 clearly show that the long-range corrections have the effect of increasing the difference between bulk vapor and liquid densities, thus, resulting in an increase in the surface tension. (2) The different treatment of LJ interactions could change the interfacial width. To illustrate this point, Fig. 6 shows 10–90 interfacial width d for both full LJ chains and chains truncated at $R_c=4$. The results clearly point at two different regimes as regards the dependence of d on R_c. At low temperature, d shows hardly any dependence on the long-range corrections, despite the increase in density differences. At high temperatures, however, the interfacial widths change dramatically with the long-range corrections.

In order to gain an understanding of the role of the long-range corrections on the surface tension, we have studied the interfacial width as a function of R_c. Figure 7 shows d as a function of the temperature, for all chains considered. Results are shown for low temperatures, well below the critical point of the untruncated fluid, $T/T_c^{\infty}\approx 0.65$ and high temperatures $T/T_c^{\infty}\approx 0.85$, not too far from the critical point. Here T_c^{∞} represents the estimation of the critical temperature of the system when the long-range corrections of the potential are included explicitly. In all cases, we observe a gradual asymptotic decrease in d as R_c is increased. (Note that interfacial widths as calculated here are smoothed by capillary fluctuations and are therefore dependent on the system's lateral size.[29,59,60] The results shown here are comparable because they are all of essentially equal area.) This behavior is a result of the broadening of the vapor-liquid equilibrium curve. For larger R_c, the density difference $\Delta\rho=\rho_L-\rho_V$ becomes larger, and hence, the interface becomes sharper. At

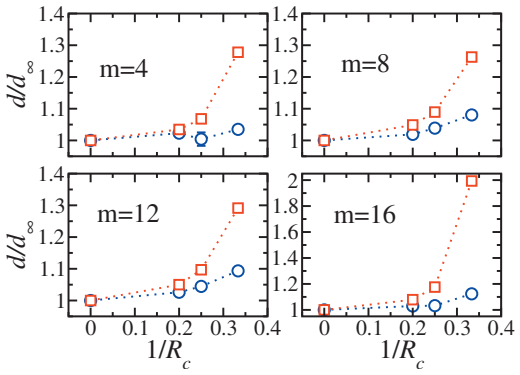

FIG. 7. Reduced interfacial thickness d/d_∞ as a function of the inverse segment-segment cutoff distance R_c for fully flexible LJ chains at two different temperatures. d_∞ is the interfacial thickness corresponding to chains interacting with a full LJ potential (including inhomogenous long-range corrections). The blue circles correspond to low temperatures (T=1.2, 1.8, 2.0, and 2.2 for m=4, 8, 12, and 16, respectively) and red squares to high temperatures (T=1.9, 2.2, 2.4, and 2.7 for m=4, 8, 12, and 16, respectively). The lines are included as a guide to the eyes.

low temperatures, the effect is small because the broadening of the coexistence curve is also small, with changes that amount to about 5% of the asymptotic value. However, for the higher temperature, the effect is quite large and noticeable (cf., full and shaded symbols in Fig. 1). The reason is that for small R_c the chains are close to their critical point $T_c(R_c)$. As a result, the interfacial thickness, which is proportional to the correlation length ξ shows an incipient divergence $\xi \sim t^{-\nu}$, with $t=1-(T/T_c)$ the reduced temperature, and ν the corresponding critical exponent.

Figure 8 shows surface tension as a function of R_c for the same two temperatures as before. Clearly, the effect of truncation is here very large both at low and high temperatures. For the low temperatures, the long-range interactions beyond $R_c=3\sigma$ account for about 40% of the asymptotic surface tension γ_∞, which has been estimated when the long-range corrections of the potential are included explicitly. Moreover, the role of the long-range corrections seems to increase with the chain length, a result that can be explained

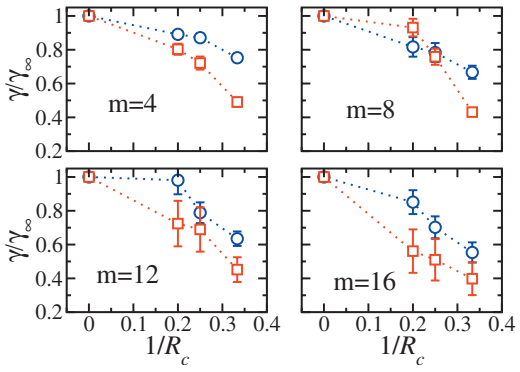

FIG. 8. Reduced surface tension γ/γ_∞ as a function of the inverse segment-segment cutoff distance R_c for fully flexible LJ chains at two different temperatures. γ_∞ is the interfacial thickness corresponding to chains interacting with a full LJ potential (including inhomogenous long-range corrections). The blue circles correspond to low temperatures (T=1.2, 1.8, 2.0, and 2.2 for m=4, 8, 12, and 16, respectively) and red squares to high temperatures (T=1.9, 2.2, 2.4, and 2.7 for m=4, 8, 12, and 16, respectively). The lines are included as a guide to the eyes.

by baring in mind the behavior of the interfacial width with the chain length. For the highest temperature, however, this may amount to even 60% of the full value. Such an important role of the long-range forces may be surprising at first thought, but can be explained by considering the behavior of the correlation length discussed earlier.

Under the square gradient approximation, the surface tension is given both at low and high temperatures by (cf. Appendix)

$$\gamma \sim C\Delta\rho^2\xi^{-1}, \tag{13}$$

where C is the square gradient coefficient, $\Delta\rho=\rho_L-\rho_V$, and ξ is the correlation length. Whereas this equation is in principle of mean field type, Widom has shown it may also be considered as a correct nonmeanfield description of γ provided the correct scaling of C, $\Delta\rho$, and ξ are incorporated *ad hoc*.[1]

At low temperatures, $\Delta\rho$ changes very little with the cutoff radius, while ξ is mainly governed by the molecular diameter and has also a weak dependence on R_c (cf. Fig. 7). Hence, the dependence of γ with R_c is mainly given by C. Using $-\beta U(r)$ as a simple approximation for the direct correlation function, we find $C(R_c)=C_\infty(1-\sigma/R_c)$.[61] Therefore, we expect

$$\gamma(R_c) = \gamma_\infty\left(1-\frac{\sigma}{R_c}\right). \tag{14}$$

Thus, the asymptotic value of the surface tension at low temperature is approached slowly.

On the other hand, at high temperatures the behavior of C, $\Delta\rho$, and ξ is no longer governed by molecular details, but rather, by scaling behavior dictated by the proximity to the fluid's critical point. Considering $C \sim t^{\eta-2\nu}$, $\Delta\rho \sim t^\beta$, and $\xi \sim t^{-\nu}$, we expect

$$\gamma(R_c) \sim \left(1-\frac{T}{T_c(R_c)}\right)^\mu, \tag{15}$$

where $\mu=\eta+2\beta-\nu$ is the scaling exponent associated to the surface tension, while β, η, and ν are the scaling exponents associated to $\Delta\rho$, the isothermal compressibility and the correlation length, respectively. In order to determine the dependence of the critical point with R_c, we consider the result of van der Waal's equation of state $T_c=[8a/27b]$ (with a the van der Waals constant, and b the covolume), whereupon we find $T_c(R_c)=T_c^\infty(1-(\sigma/R_c)^3)$. Therefore, the dependence of γ on R_c at high temperatures becomes

$$\gamma(R_c) = \gamma_\infty\left(1-\frac{T}{T_c^\infty - T}\left(\frac{\sigma}{R_c}\right)^3\right)^\mu. \tag{16}$$

This equation shows (i) that the increase in γ with R_c is steeper close to the critical point of the untruncated LJ fluid, (ii) $\gamma(R_c)$ vanishes eventually when $(R_c/\sigma)^3$ becomes equal to $T/(T_c^\infty-T)$, i.e., when T becomes equal to the critical temperature of the truncated LJ fluid. Hence, for temperatures close enough to $T_c(R_c)$, the "long-range corrections" to the surface tension can be as large as 100% of the full value, although this is simply a trivial effect due to the lower critical point of the fluid with truncated interactions.

Having studied the role of long-range corrections, let us now discuss the chain length dependence of interfacial properties. Inspection of Fig. 5 shows that for a constant temperature, the surface tension increases as the chain length increases. This is not surprising, in view of the increasing segregation $\Delta\rho$ with the chain length (cf. Fig. 3). Similar to $\Delta\rho$, however, the surface tension exhibits an apparently asymptotic behavior, leading to chain length independent surface tensions for large enough degree of polymerization. Such results are consistent with experimental evidence based on, e.g., the homologous series of polydimethylsiloxane at room temperature[62] and with theoretical considerations.[29,35,63] The chain length dependence for finite chains is less clear. Thompson *et al.*[63] have recently studied this issue and found a dependence with m of the form $\gamma(m)=\gamma_\infty(1-m^{-\lambda})$, with $\lambda=2/3$ for short chains and $\lambda=1$ for long chains. We have checked that our results are consistent with the suggested power law, but unfortunately do not have data of sufficient quality to extract a meaningful exponent (fits of γ to m^{-1} and $m^{-2/3}$ are both of similar good quality).

The asymptotic behavior of $\gamma(m)$ should be the results of two asymptotic behaviors that govern the surface tension as the chain length increases, one due to the segregation, and the other due to the behavior of the interfacial thickness as a function of m.[60] The asymptotic behavior of the polymer segregation at low temperatures is a well known fact and can be explained on the basis of Flory–Huggins theory or TPT1 (cf. Ref. 47). Whether the interfacial thickness shows an asymptotic behavior is *a priori* less clear because one cannot rule out whether the relevant length scale is a monomer property or the polymer radius of gyration. The results of Fig. 6 clearly suggest the attainment of an asymptotic behavior, of similar form as that observed for the surface tension or polymer segregation. This observation is consistent with theoretical predictions based on a square gradient approximation for polymers, which suggest that the interfacial thickness for long enough polymers depends only on the liquid coexistence density and the statistical segment length.[29]

V. CONCLUSIONS

In this work we have studied the interfacial properties of freely jointed LJ chains with effectively untruncated interactions. We have paid particular attention to two important points.

First, we have considered the role of truncated LJ interactions. We have found that the method employed for the calculation of long-range corrections to the energy is a viable and robust methodology.[14,16] Furthermore, we have shown that the long-range corrections may be written in the form of an effective long-range pair potential. Whereas explicit evaluation of such potential makes the simulations more time consuming, it can be readily implemented into a simulation code without the need to update an instantaneous density profile every move. Using a truncation sphere at $R_c=3\sigma$ plus effective long-range pair potential takes about the same time than a simulation of truncated pair potential at $R_c=4\sigma$, but the former provides a much better converged result of the full LJ potential. Therefore, the effective pair potential proposed here is indeed a viable alternative for problems where cpu time is not a critical issue. We have shown that neglected LJ interactions beyond typical cutoff values such as $R_c=4\sigma$ may account for as much as 40% of the surface tension, and even more so for higher temperatures, where the depressed critical point of the truncated model leads to a very rapid decrease in the surface tension. Furthermore, the role of the long-range interactions becomes more important as the chain length is increased.

Second, we have studied the chain length dependence of interfacial properties of the LJ chains with untruncated potential. The results show that the surface tension increases with chain length toward an asymptotic value, while the interfacial width has the opposite trend, decreasing toward an asymptotic value as the chain length increases. The somewhat unexpected decrease in d with chain length is explained easily as a trivial equation of state effect: as chain length increases, the corresponding states temperature decreases due to the increase in the critical temperature. Hence, at a given temperature the long chain is further away from its critical point and exhibits a sharper interface. This equation of state effect has a more prominent role than the increase in the polymer's radius of gyration, which seems to play a minor role in the shape of the interface.

ACKNOWLEDGMENTS

We wish to acknowledge helpful discussions with E. de Miguel, G. Jackson, and C. Vega and P. Bryk. This work was supported by Ministerio de Educacion y Ciencia through Grant Nos. FIS2007-66079-C02-01 and FIS2007-66079-C02-02. Further financial support from projects PR34/07-15906 (Santander-UCM), CCG08-UCM/ESP-4358 (CAM–UCM), MOSSNOHO-S0505/ESP/0299 (CAM), and P07-FQM02884 (Junta de Andalucía) is also acknowledged. One of us (F.J.B.) also thanks Universidad de Huelva for additional support.

APPENDIX: PROVE OF EQUATION (13)

According to the square gradient theory, the surface tension is

$$\gamma=\int_{-\infty}^{\infty}C(\rho)\left(\frac{d\rho}{dz}\right)^2dz. \tag{A1}$$

Considering C a constant and the hyperbolic tangent approximation for the density profile $\rho=\rho(z)$, we get

$$\gamma=\frac{C\Delta\rho^2}{16}\int_{-\infty}^{\infty}\left[1-\tanh^2\left(\frac{1}{2}\frac{z}{\xi}\right)\right]^2dz, \tag{A2}$$

where $\Delta\rho=\rho_l-\rho_v$ and ξ is the correlation length. The integrand may be approximated to a Gaussian (the series expansion is equal up to second order and very nearly equal up to fourth order), which, after integration, yields Eq. (13).

[1] J. Rowlinson and B. Widom, *Molecular Theory of Capillarity* (Clarendon, Oxford, 1982).
[2] M. Allen and D. Tildesley, *Computer Simulation of Liquids* (Clarendon, Oxford, 1987).
[3] D. P. Landau and K. Binder, *A Guide to Monte Carlo Simulations in*

Statistical Physics (Cambridge University Press, Cambridge, England, 2000).
[4] B. J. Alder and T. E. Wainright, J. Chem. Phys. **27**, 1208 (1957).
[5] W. Wood and J. D. Jacobson, J. Chem. Phys. **27**, 1207 (1957).
[6] J. E. Mayer and W. W. Wood, J. Chem. Phys. **42**, 4268 (1965).
[7] K. Binder, Phys. Rev. A **25**, 1699 (1982).
[8] P. Orea, Y. Duda, and J. Alejandre, J. Chem. Phys. **123**, 114702 (2005).
[9] A. Trokhymchuk and J. Alejandre, J. Chem. Phys. **111**, 8510 (1999).
[10] G. A. Chapela, G. Saville, S. M. Thompson, and J. S. Rowlinson, J. Chem. Soc., Faraday Trans. **73**, 1133 (1977).
[11] J. Lopez-Lemus, M. Romero-Bastida, T. A. Darden, and J. Alejandre, Mol. Phys. **104**, 2413 (2006).
[12] M. Guo and B. C.-Y. Lu, J. Chem. Phys. **106**, 3688 (1997).
[13] M. Mecke, J. Winkelmann, and J. Fischer, J. Chem. Phys. **107**, 9264 (1997).
[14] J. Janeček, H. Krienke, and G. Schmeer, J. Phys. Chem. B **110**, 6916 (2006).
[15] K. F. Mansfield and D. N. Theodorou, Macromolecules **23**, 4430 (1990).
[16] K. C. Daoulas, V. A. Harmandaris, and V. G. Mavrantzas, Macromolecules **38**, 5780 (2005).
[17] F. Biscay, A. Ghoufi, F. Goujon, V. Lachet, and P. Malfreyt, J. Chem. Phys. **130**, 184710 (2009).
[18] E. M. Blokhuis, D. Bedeaux, C. D. Holcomb, and J. A. Zollweg, Mol. Phys. **85**, 665 (1995).
[19] F. Goujon, P. Malfreyt, A. Boutin, and A. H. Fuchs, J. Chem. Phys. **116**, 8106 (2002).
[20] C. Vega and L. G. MacDowell, J. Chem. Phys. **126**, 154707 (2007).
[21] A. Ghoufi, F. Goujon, V. Lachet, and P. Malfreyt, J. Chem. Phys. **128**, 154716 (2008).
[22] C. Ibergay, A. Ghoufi, F. Goujon, P. Ungerer, A. Boutin, B. Rousseau, and P. Malfreyt, Phys. Rev. E **75**, 051602 (2007).
[23] J. Janeček, J. Phys. Chem. B **110**, 6264 (2006).
[24] M. Mecke, J. Winkelmann, and J. Fischer, J. Chem. Phys. **110**, 1188 (1999).
[25] F. Bresme, E. Chacon, P. Tarazona, and K. Tay, Phys. Rev. Lett. **101**, 056102 (2008).
[26] N. Karasawa and W. Goddard, J. Phys. Chem. **93**, 7320 (1989).
[27] V. K. Shen, R. D. Mountain, and J. R. Errington, J. Phys. Chem. B **111**, 6198 (2007).
[28] F. J. Blas, L. G. MacDowell, E. de Miguel, and G. Jackson, J. Chem. Phys. **129**, 144703 (2008).
[29] M. Müller and L. G. MacDowell, Macromolecules **33**, 3902 (2000).
[30] A. Milchev and K. Binder, J. Chem. Phys. **114**, 8610 (2001).
[31] F. Varnik, J. Baschnagel, and K. Binder, J. Chem. Phys. **113**, 4444 (2000).
[32] D. Duque, J. C. Pamies, and L. F. Vega, J. Chem. Phys. **121**, 11395 (2004).
[33] P. Virnau, M. Müller, L. MacDowell, and K. Binder, J. Chem. Phys. **121**, 2169 (2004).
[34] B. M. Mognetti, L. Yelash, P. Virnau, W. Paul, K. Binder, M. Mueller, and L. G. MacDowell, J. Chem. Phys. **130**, 044101 (2009).
[35] P. Bryk, K. Bucior, S. Sokolowski, and G. Zukocinski, J. Phys.: Condens. Matter **16**, 8861 (2004).
[36] L. G. MacDowell and P. Bryk, Phys. Rev. E **75**, 061609 (2007).
[37] G. J. Gloor, G. Jackson, F. J. Blas, and E. de Miguel, J. Chem. Phys. **123**, 134703 (2005).
[38] R. D. Mountain, J. Phys. Chem. B **113**, 482 (2009).
[39] L. G. MacDowell, Ph.D. thesis, Universidad Complutense de Madrid, 2000.
[40] L. G. MacDowell, C. Vega, and E. Sanz, J. Chem. Phys. **115**, 6220 (2001).
[41] J. I. Siepmann and D. Frenkel, Mol. Phys. **75**, 59 (1992).
[42] E. de Miguel, J. Phys. Chem. B **112**, 4674 (2008).
[43] L. G. MacDowell, M. Müller, C. Vega, and K. Binder, J. Chem. Phys. **113**, 419 (2000).
[44] A subtle point that might have passed unnoticed is that the results only agree to order L_z^{-3} because of the neglect of long-range interactions beyond L_z in Janeček's method. Whereas such a correction is completely negligible in usual simulation setups, where L_z is several decades long in units of σ, the difference is measurable in bulk systems with $L_z=10\sigma$.
[45] F. A. Escobedo and J. J. de Pablo, Mol. Phys. **87**, 347 (1996).
[46] M. S. Wertheim, J. Chem. Phys. **87**, 7323 (1987).
[47] C. Vega, F. J. Blas, and A. Galindo, J. Chem. Phys. **116**, 7645 (2002).
[48] K. Binder, Z. Phys. B **43**, 119 (1981).
[49] N. B. Wilding, Phys. Rev. E **52**, 602 (1995).
[50] W. G. Chapman, G. Jackson, and K. E. Gubbins, Mol. Phys. **65**, 1057 (1988).
[51] C. Vega and L. G. MacDowell, Mol. Phys. **98**, 1295 (2000).
[52] J. K. Johnson, E. A. Muller, and K. E. Gubbins, J. Phys. Chem. **98**, 6413 (1994).
[53] F. J. Blas and L. F. Vega, Mol. Phys. **92**, 135 (1997).
[54] Y. Tang and B. C.-Y. Lu, Fluid Phase Equilib. **190**, 149 (2001).
[55] J. K. Johnson, J. Chem. Phys. **104**, 1729 (1996).
[56] F. Blas and L. Vega, J. Chem. Phys. **115**, 4355 (2001).
[57] K. G. Honnell, C. K. Hall, and R. Dickman, J. Chem. Phys. **87**, 664 (1987).
[58] L. G. MacDowell, J. Chem. Phys. **119**, 453 (2003).
[59] E. Chacon and P. Tarazona, J. Phys.: Condens. Matter **17**, S3493 (2005).
[60] C. Carelli, R. A. L. Jones, R. N. Young, R. Cubitt, R. Dalgliesh, F. Schmid, and M. Sferrazza, Phys. Rev. E **72**, 031807 (2005).
[61] As an opposite limiting case we may consider the sharp-kink approximation for the interface profile. The decay towards the asymptotic value is then or order R_c^{-2}. Most likely, the decay may be described as R_c^n, with n between 1 and 2.
[62] P. G. de Gennes, F. Brochard-Wyart, and D. Quéré, *Capillarity and Wetting Phenomena* (Springer, New York, 2004).
[63] R. B. Thompson, J. R. MacDonald, and P. Chen, Phys. Rev. E **78**, 030801 (2008).